

# S-MATRIX POLES CLOSE TO THRESHOLDS IN CONFINED GEOMETRIES

Giorgio Cattapan

*Dipartimento di Fisica “G. Galilei”, Università di Padova,  
Via F. Marzolo 8, I-35131 Padova, Italy  
Istituto Nazionale di Fisica Nucleare, Sezione di Padova,  
Via F. Marzolo 8, I-35131 Padova, Italy*

Paolo Lotti

*Istituto Nazionale di Fisica Nucleare, Sezione di Padova,  
Via F. Marzolo 8, I-35131 Padova, Italy  
Dipartimento di Fisica “G. Galilei”, Università di Padova,  
Via F. Marzolo 8, I-35131 Padova, Italy*

## Abstract

We have studied the behavior of the  $S$ -matrix poles near threshold for quantum waveguides coupled to a cavity with a defect. We emphasize the occurrence of both dominant and shadow poles on the various sheets of the energy Riemann surface, and show that the changes of the total conductivity near threshold as the cavity's width changes can be explained in terms of dominant to shadow pole transitions.

PACS numbers: 73.63.Nm Quantum wires, 73.23.Ad Ballistic transport, 72.10.Fk Scattering by point defects, dislocations, surfaces, and other imperfections (including Kondo effect)

Preprint DFPD/07/TH12

In multichannel scattering, the poles of the  $S$ -matrix lie in general on different sheets of the Riemann energy surface. Poles on the negative real axis of the physical sheet correspond to bound states of the system, while poles on the unphysical sheets close to the physical energy axis are associated to resonant states. In addition to the resonance, *dominant* poles, however, there are also poles on unphysical sheets, far away from the physical region, which do not have in general observable effects, and have been referred to as *shadow* poles [1]. The possible role of shadow poles has been discussed over the years in the context of particle [2], nuclear [3] and atomic [4] physics, as well as in laser-induced multiphoton processes [5, 6]. Their study is of particular relevance when the scattering process depends upon some tunable parameter; as this parameter is changed, the  $S$ -matrix poles move on the various sheets of the energy Riemann surface, and may pass a scattering threshold. In so doing, some shadow pole may approach the physical region, thereby becoming dominant, and producing observable effects, whereas a previously dominant pole may retire to a less exposed position [7].

In this paper we would like to point out another situation, where shadow and dominant poles may exchange their roles, and give rise to non-trivial observable effects near threshold. It stems from recent developments in nanotechnology, which allow one to obtain a strictly two-dimensional electron gas subject to confined geometries [8, 9]. To be definite, we shall consider the device of Fig. 1, where a resonant cavity or stub having width  $c$  and length  $l_s$  is coupled to a uniform guide of indefinite length and width  $b$ . The stub contains a region, depicted by the shaded area in Fig. 1, with a defect described by a potential field  $V(x, y)$ . For high-purity materials and at low temperatures, the electron's motion inside the duct is ballistic, and can be described as a scattering process [8, 9], the conductivity of the quantum circuit being expressible in term of the transmission coefficients of the system.

Recently, we have developed an  $S$ -matrix approach to stubbed wave guides with defects, which allows for an accurate numerical solution of the scattering problem even when some critical dimension of the system gets large [10]. We start from the two-dimensional Schrödinger equation

$$\left\{ -\frac{\hbar^2}{2m^*} \nabla_2^2 + V(x, y) \right\} \Psi(x, y) = E \Psi(x, y) \quad , \quad (0.1)$$

where  $\nabla_2^2$  is the two-dimensional Laplace operator,  $E$  the total energy, and  $m^*$  represents the effective mass of the electron in the conduction band. Assuming hard-wall boundary

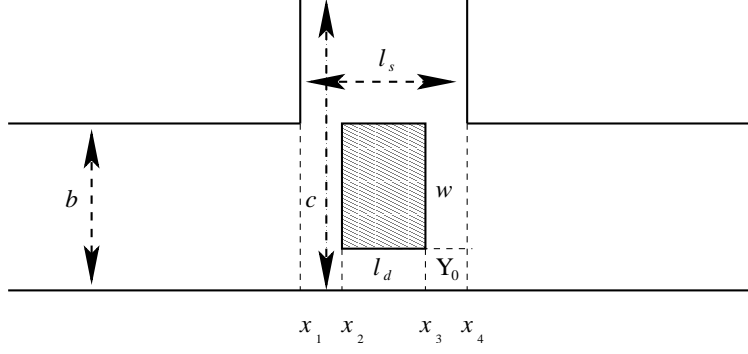


FIG. 1: A stubbed quantum waveguide of width  $b$  and infinite length, with a stub of width  $c$  and length  $l_s$ . The stub contains a defect with dimensions  $w \times l_d$ .

conditions, the total wave function  $\Psi(x, y)$  is expanded in terms of the transverse mode eigenfunctions in the lead and in the cavity, and the Schrödinger equation (0.1) is replaced by an (in principle) infinite set of coupled, one-dimensional Schrödinger equations. The latter can be reduced to linear, algebraic equations matching the wave function and its first derivative at the various interfaces delimiting the duct from the cavity, and the empty part of the cavity from the region where the potential acts. Thus, the scattering operator for each segment in the quantum circuit can be evaluated through linear algebra. The total  $S$ -matrix of the device is finally obtained from the partial scattering operators by recursively applying the  $\star$ -product composition rule, which expresses the overall scattering matrix  $\mathbf{S}$  in terms of the partial scattering matrices  $\mathbf{S}^{(a)}$  and  $\mathbf{S}^{(b)}$  as [8, 10]

$$\mathbf{S} = \begin{pmatrix} \mathbf{S}_{11} & \mathbf{S}_{12} \\ \mathbf{S}_{21} & \mathbf{S}_{22} \end{pmatrix} = \mathbf{S}^{(a)} \star \mathbf{S}^{(b)} \quad , \quad (0.2)$$

where

$$\mathbf{S}_{11} = \mathbf{S}_{11}^{(a)} + \mathbf{S}_{12}^{(a)} \mathbf{S}_{11}^{(b)} \left( \mathbf{1} - \mathbf{S}_{22}^{(a)} \mathbf{S}_{11}^{(b)} \right)^{-1} \mathbf{S}_{21}^{(a)} \quad , \quad (0.3a)$$

$$\mathbf{S}_{12} = \mathbf{S}_{12}^{(a)} \left( \mathbf{1} - \mathbf{S}_{11}^{(b)} \mathbf{S}_{22}^{(a)} \right)^{-1} \mathbf{S}_{12}^{(b)} \quad , \quad (0.3b)$$

$$\mathbf{S}_{21} = \mathbf{S}_{21}^{(b)} \left( \mathbf{1} - \mathbf{S}_{22}^{(a)} \mathbf{S}_{11}^{(b)} \right)^{-1} \mathbf{S}_{21}^{(a)} \quad , \quad (0.3c)$$

$$\mathbf{S}_{22} = \mathbf{S}_{22}^{(b)} + \mathbf{S}_{21}^{(b)} \mathbf{S}_{22}^{(a)} \left( \mathbf{1} - \mathbf{S}_{11}^{(b)} \mathbf{S}_{22}^{(a)} \right)^{-1} \mathbf{S}_{12}^{(b)} \quad . \quad (0.3d)$$

Because of the presence of forward propagating modes only, the evaluation of the scattering matrix is numerically stable also for “large” systems. Moreover, the composition rule (0.2)

naturally accommodates a different number of modes in the lead and in the cavity. These features are of particular relevance in the present instance, where the stub's width  $c$  may vary over a rather large range of values [10].

It is worth to stress here that each block  $\mathbf{S}_{ij}$  in the scattering operator  $\mathbf{S}$  is itself a matrix, whose elements are labeled by mode or channel indexes. For an incoming wave of unit flux impinging from the left,  $(\mathbf{S}_{11})_{nm}$  represents the reflection coefficient towards the left from the initial channel  $m$  into the final one  $n$ , whereas  $(\mathbf{S}_{21})_{nm}$  is the transmission coefficient to the right from mode  $m$  into mode  $n$ . Similarly,  $(\mathbf{S}_{12})_{nm}$  and  $(\mathbf{S}_{22})_{nm}$  are the  $m \rightarrow n$  transmission amplitudes to the left and reflection coefficient to the right for an electron incoming from the right. Once the transmission coefficients are known, the total conductance  $G$  (in units  $2e^2/h$ ) is given by the Büttiker formula [8, 9, 11]

$$G = \sum_{m,n} \frac{k_n^{(l)}}{k_m^{(l)}} |(\mathbf{S}_{21})_{nm}|^2, \quad (0.4)$$

where  $k_n^{(l)}$  and  $k_m^{(l)}$  denote the lead propagation momenta in channel  $n$  and  $m$ , respectively, and the sum is restricted to the open channels in the duct.

The above  $S$ -matrix approach can be straightforwardly extended to complex energies. We used our code to numerically locate the poles of the  $S$ -matrix in the multi-sheeted energy surface. In the following, sheets will be specified according to the sign of the imaginary part of the lead momenta in the various channels [12]. Thus, for a four-channel situation, the physical sheet, where all the imaginary parts of the momenta are positive, will be denoted as  $(++++)$ , whereas on the sheet  $(-+++)$  one has  $\text{Im}k_1^{(l)} < 0$  and  $\text{Im}k_i^{(l)} > 0$  for the other three channels. Dominant poles producing resonance effects in the lowest subband, between the first and second scattering thresholds  $E_T^{(1)}$  and  $E_T^{(2)}$ , are in the fourth quadrant of this sheet near the real energy axis, and have  $E_T^{(1)} \leq \text{Re}E_p \leq E_T^{(2)}$ . Similarly, dominant poles for resonances in the second subband with  $E_T^{(2)} \leq E \leq E_T^{(3)}$  lie in sheet  $(--++)$  and have  $E_T^{(2)} \leq \text{Re}E_p \leq E_T^{(3)}$ . We have chosen the value  $m^* = 0.067m_e$  for the effective electron mass, which is appropriate for the  $\text{Al}_x\text{Ga}_{1-x}\text{As}/\text{GaAs}$  interface. We verified that convergence is attained for both the conductance and the pole positions when four channels are included in the external duct, and up to ten channels are taken into account in the cavity. In these conditions, the position of the poles in the complex energy plane can be guaranteed with an accuracy of the order  $10^{-5}$ . From now on, to exploit the scale invariance of the system, all lengths are measured in terms of the waveguide width  $b$ , and energies in terms of the

waveguide fundamental mode  $\epsilon_1^{(l)} = \frac{\hbar^2}{2m^*} \left(\frac{\pi}{b}\right)^2$ , and the “tilde” symbol will be used to denote adimensional quantities, so that one has for the various thresholds  $\tilde{E}_T^{(n)} = 1, 2, \dots$ . The calculations we present refer to a device with  $\tilde{l}_s = 1$ ; a repulsive, double Gaussian defect

$$\tilde{V}(\tilde{x}, \tilde{y}) \equiv \tilde{V}_0 e^{-\tilde{\beta}^2(\tilde{x}-\tilde{x}_c)^2 - \tilde{\alpha}^2(\tilde{y}-\tilde{y}_c)^2} \quad (0.5)$$

centered in  $(\tilde{x}_c, \tilde{y}_c) = (0.50, 0.25)$  has been allowed in the cavity. The decay constants along the transverse and propagation direction have been fixed at  $\tilde{\alpha} = 15$ ,  $\tilde{\beta} = 10$ , so as to ensure that the potential is entirely contained within a region  $\tilde{w} = 0.3$  wide and  $\tilde{l}_d = 1$  long, displaced a distance  $\tilde{Y}_0 = 0.1$  from the lower edge of the guide. The smooth dependence of  $\tilde{V}(\tilde{x}, \tilde{y})$  has been taken into account through a slicing technique, *i.e.*, replacing the actual interaction with a sequence of pseudodefects having a constant value along the  $x$  direction [10, 13]. Quite stable results are obtained with  $N = 10 \div 15$  slices. In the present calculations we have chosen  $\tilde{V}_0 = 4$ .

In Fig. 2 we report the trajectories on the complex energy surface of three  $S$ -matrix poles with varying stub's width  $\tilde{c}$ . Pole 1 moves from the upper edge  $\tilde{E}_T^{(2)}$  towards the lower edge  $\tilde{E}_T^{(1)}$  of the first subband as  $\tilde{c}$  is increased from 1.50 to 5.00. Similarly, pole 2 moves downwards from the third threshold passing below the second one as  $\tilde{c}$  is increased from  $\tilde{c} = 1.00$  up to  $\tilde{c} = 2.00$ , whereas pole 3 refer to  $1.33 \leq \tilde{c} \leq 5.00$ . In all cases one has the “binding” effect typical of an increase of the stub's width [10]. Note that the three pole trajectories appear to be close to each other, but are in fact on different sheets of the energy Riemann surface. Pole 1 lies on the  $(-+++)$  sheet, and can produce resonance effects in the first subband, whereas poles 2 and 3 belong to the  $(--++)$  sheet, and are responsible of resonance structures in the second subband. As a consequence, pole 2 is a dominant pole until it passes below  $E_T^{(2)}$ , which happens for  $\tilde{c} = 1.54$ ; for  $\tilde{c} > 1.54$  it becomes a shadow pole, since the  $(--++)$  sheet is more distant from the first subband than the  $(-+++)$  sheet, where the relevant resonance poles may be found. Similarly, pole 3 is shadow for  $\tilde{c} < 2.40$ , and becomes a dominant pole for greater values of  $\tilde{c}$ . In Fig. 2 dominant and shadow poles are drawn as full and dashed lines, respectively.

The change of status of a pole from dominant to shadow pole as it passes a threshold can explain the remarkable effects that even small variations of  $\tilde{c}$  may have on the conductance near threshold. This is illustrated in Fig. 3, where we plot the conductance in the second threshold region ( $3.5 \leq \tilde{E} \leq 4.5$ ), in correspondence to  $\tilde{c} = 1.520, 1.540, 1.541$ , and  $1.560$ .

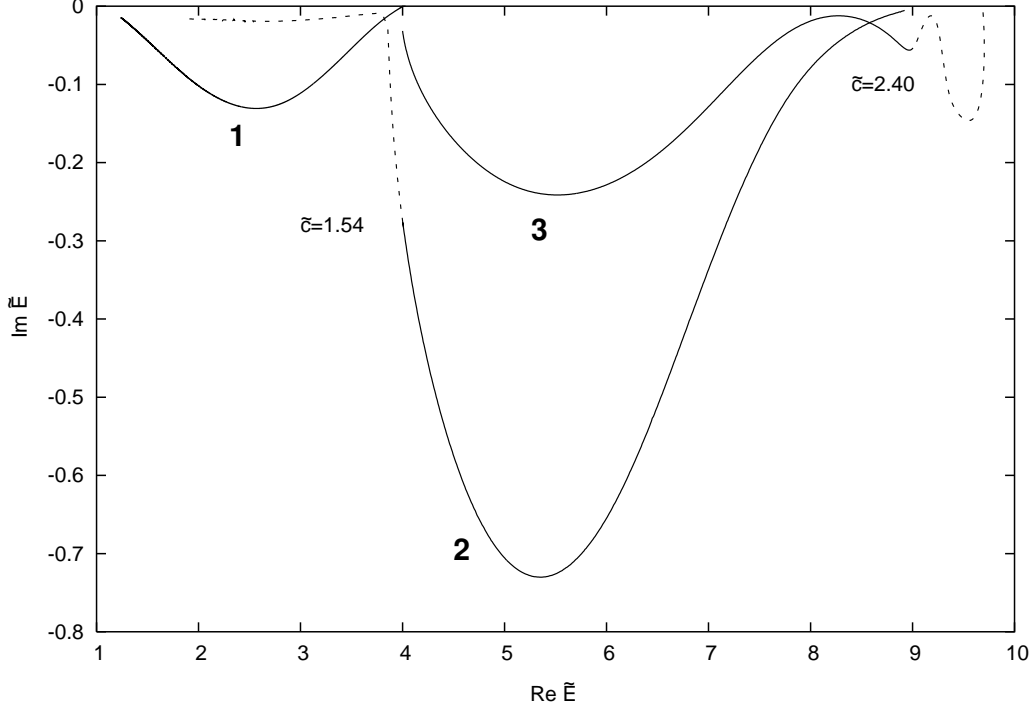


FIG. 2: Motion of three  $S$ -matrix poles on the Riemann energy surface with varying  $\tilde{c}$ . The three trajectories correspond to  $1.50 \leq \tilde{c} \leq 5.00$ ,  $1.00 \leq \tilde{c} \leq 2.00$ , and  $1.33 \leq \tilde{c} \leq 5.00$  for pole 1, 2, and 3, respectively. Note that pole 1 moves on the  $(-+++)$  sheet, whereas poles 2 and 3 belong to the  $(--++)$  sheet. Shadow and dominant poles are drawn as dashed and full lines, respectively. The values of  $\tilde{c}$  where a pole changes its nature are given in the figure.

The corresponding conductance profiles are given by the solid, long-dashed, short-dashed, and dotted lines, respectively.

For  $\tilde{c} = 1.520$  pole 2 is dominant, since one has  $\tilde{E}_p \simeq 4.14 - 0.39i$ , and produces the resonance peak one observes just above threshold. For  $\tilde{c} = 1.540$  and  $\tilde{c} = 1.541$  pole 2 is just above ( $\tilde{E}_p \simeq 4.002 - 0.276i$ ) and just below ( $\tilde{E}_p \simeq 3.990 - 0.270i$ ) threshold. One has that the resonance peak is still visible in both cases, which means that the dominant  $\rightarrow$  shadow transition does not prevent the pole from having effects on the observable quantities. For  $\tilde{c} = 1.560$  the pole has moved down to  $\tilde{E}_p \simeq 3.87 - 0.09i$ , and it is far away enough from the physical region, to have no effects on the conductance, which appears rather flat above threshold. It is worth to stress that for these values of  $\tilde{c}$  pole 1 is far above the second threshold, and cannot influence the conductance profile in the first subband; as a matter of fact, in all cases the conductance is practically the same below threshold, and exhibits a cusp

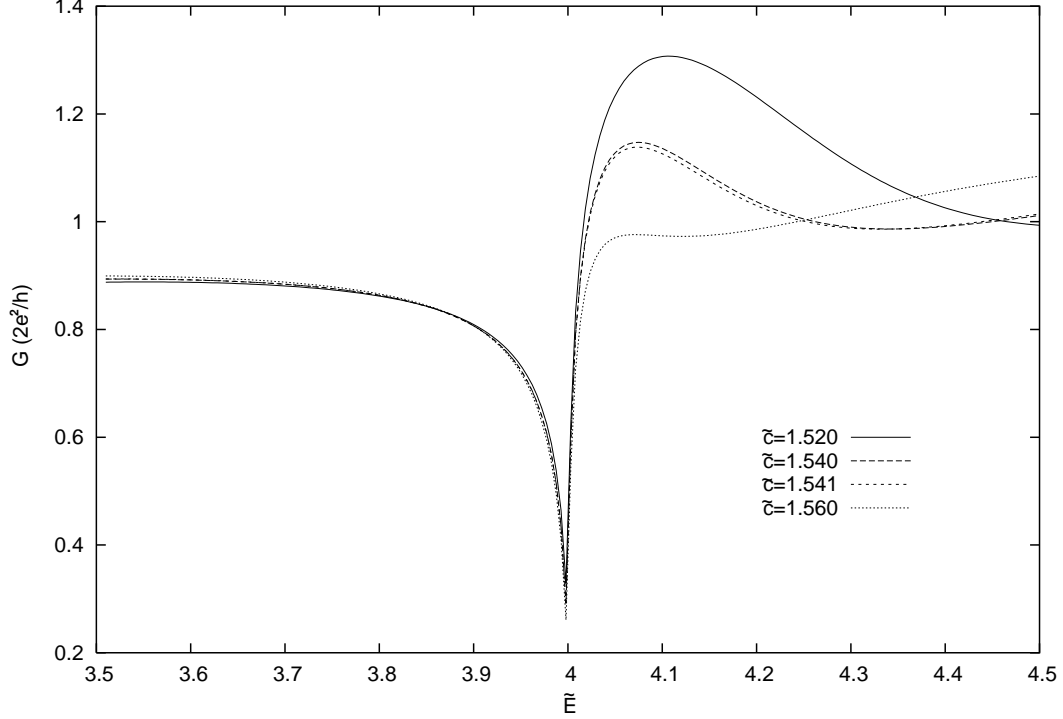


FIG. 3: Conductance (in units  $2e^2/h$ ) in the region of the second threshold for  $\tilde{c} = 1.520$  (solid line),  $\tilde{c} = 1.540$  (dashed line),  $\tilde{c} = 1.541$  (short-dashed line), and  $\tilde{c} = 1.560$  (dotted line).

structure, with infinite slope as a function of energy both from above and from below. This behavior is indeed discernible at threshold in all calculations, and can be explained much in the same way, as one explains threshold phenomena in inelastic scattering processes. When a new transverse mode opens up, less energy is available in the propagation direction, so that one has the analogue of “endoergic” reactions in inelastic scattering [7]. From Eq. (0.4) one sees that  $G$  is linear with respect to the corresponding final momentum  $k_n^{(l)}$ . Since  $k_n^{(l)}$  is related to the total energy  $E$  and to the relevant waveguide eigenenergy  $\epsilon_n^{(l)}$  by [10]

$$k_n^{(l)} = [2m^* (E - \epsilon_n^{(l)}) / \hbar^2]^{1/2} ,$$

one actually expects an infinite derivative of  $G$  with respect to  $E$  [7].

The effects due to the exchange of role between shadow and dominant poles are illustrated in Fig. 3, where we plot  $G$  near the second threshold for  $\tilde{c} = 1.54$  (solid line) and  $\tilde{c} = 1.70$  (dashed line). In the former case one has the resonance peak above threshold due to pole 2, as discussed previously; in the latter, pole 2 has moved down to  $\tilde{E}_p \simeq 2.68 - 0.02i$  and has no effect on the conductance any longer; pole 1 which moves on the  $(-+++)$  sheet, on the other hand, is now dominant, being located at  $\tilde{E}_p \simeq 3.78 - 0.02i$ , and produces the Fano

dip one observes in Fig. 3. Note that in the first subband one can have the simultaneous presence of poles and transmission zeros, which cannot occur when more than a propagating mode are active.

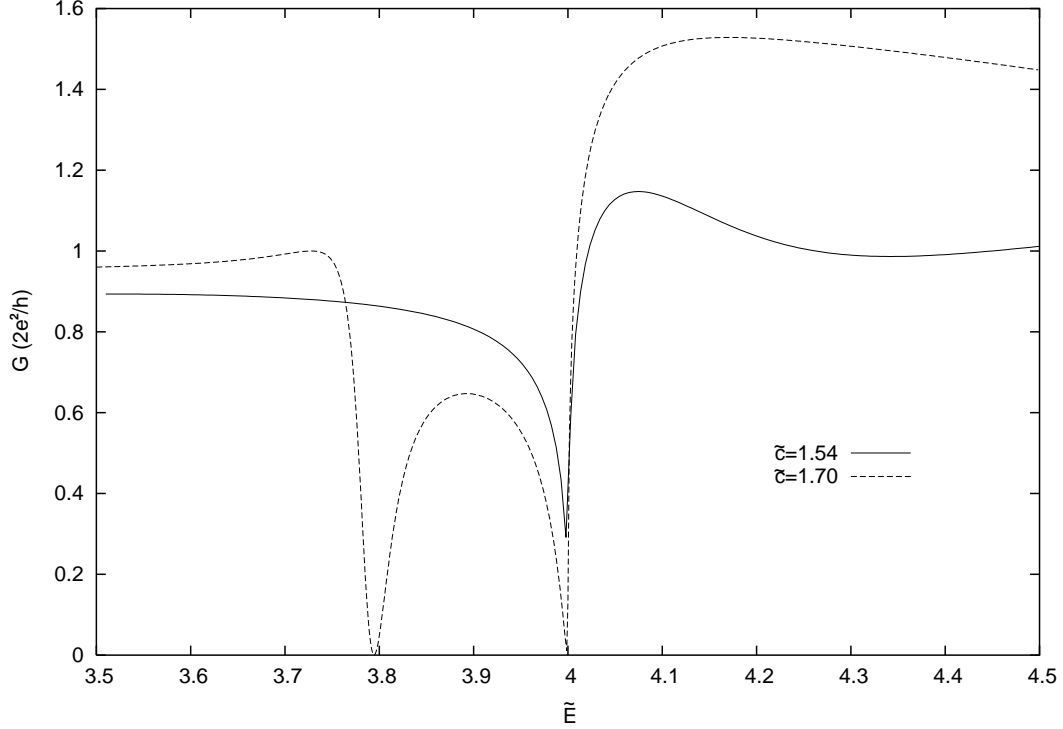


FIG. 4: Conductance (in units  $2e^2/h$ ) in the region of the second threshold for  $\tilde{c} = 1.54$  (solid line) and  $\tilde{c} = 1.70$  (dashed line).

A similar phenomenon is visible in correspondence to the third threshold. An example is given in Fig. 5, where the conductance around the third threshold is plotted for  $\tilde{c} = 2.37$  and  $\tilde{c} = 2.42$ . While a resonance dip is clearly visible in the latter case, no resonance at all is discernible for the shorter stub, and only the threshold cusp survives for the conductance profile. Such a striking change in correspondence to so small a change in the cavity width can be readily explained in terms of a dominant to shadow pole transition. Indeed, for  $\tilde{c} = 2.42$  pole 3 of Fig. 2 is located at  $\tilde{E}_p \simeq 8.92 - 0.053i$  in the  $(- - ++)$  sheet, and plays the role of dominant pole for the second subband. When the stub is shortened, the pole moves on its sheet up to  $\tilde{E}_p \simeq 9.11 - 0.023i$ , in correspondence to the third subband, and becomes a shadow pole.

In conclusion, we have demonstrated that the behavior of the conductance near the thresholds for the opening of new propagating modes, and its sometimes striking changes in



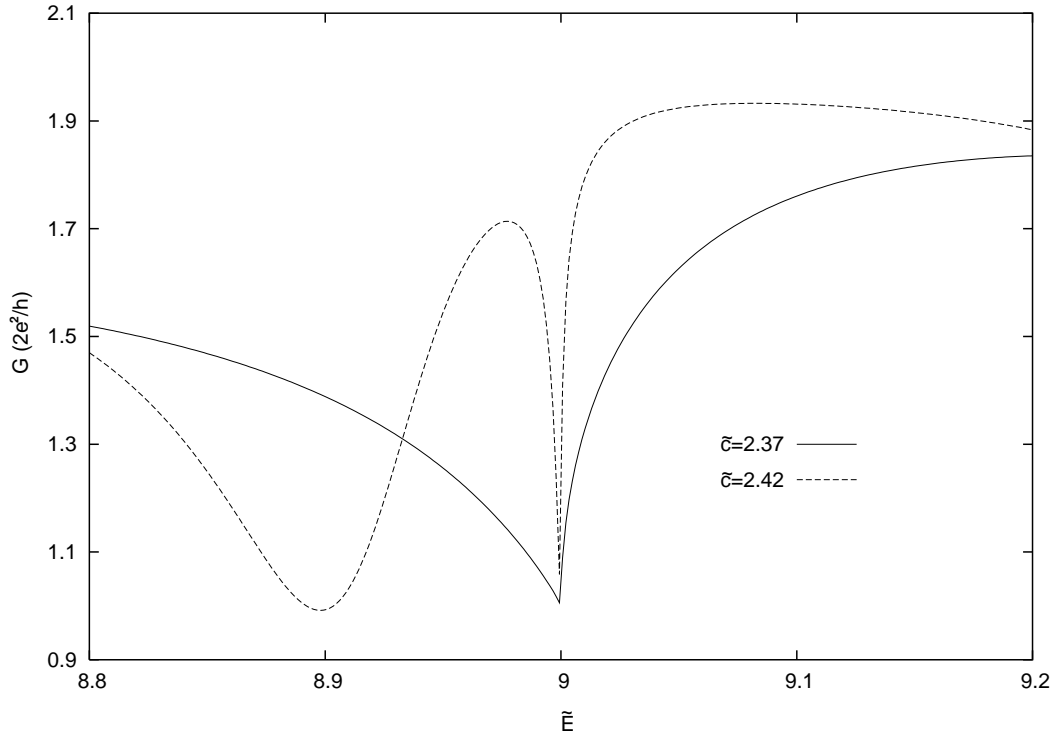


FIG. 5: Conductance (in units  $2e^2/h$ ) in the region of the third threshold for  $\tilde{c} = 2.37$  and  $\tilde{c} = 2.42$ .

correspondence to moderate or even small variations of the stub's width are signals of the transition from a dominant to a shadow status of the  $S$ -matrix poles. This result shows that concepts and methods of the analytic  $S$ -matrix, widely employed in traditional scattering theory, may have their counterpart in the analysis of systems with a confined geometry.

- 
- [1] R. J. Eden and J. R. Taylor, Phys. Rev. **133 B**, 1575 (1964)
  - [2] Y. Fujii and M. Fukugita, Nucl. Phys. B **85**, 179 (1975)
  - [3] R. E. Brown, N. Jarmie, and G. M. Hale, Phys. Rev. C **35**, 1999 (1987)
  - [4] A. Herzenberg and D. Ton-That, J. Phys. B **8**, 426 (1975)
  - [5] R. M. Potvliege and R. Shakeshaft, Phys. Rev. A **38**, 6190 (1988)
  - [6] M. Dörr and R. M. Potvliege, Phys. Rev. A **41**, 1472 (1990).
  - [7] R. G. Newton, *Scattering Theory of Waves and Particles* (Springer, New York, 1982)
  - [8] S. Datta, *Electronic Transport in Mesoscopic Systems* (Cambridge University Press, Cambridge, 1995)
  - [9] D. K. Ferry and S. M. Goodnick, *Transport in Nanostructures* (Cambridge University Press,

Cambridge, 1997)

- [10] G. Cattapan and P. Lotti, *Fano resonances in stubbed quantum waveguides with impurities*, preprint DFPD/07/TH11
- [11] R. Büttiker, Y. Imry, R. Landauer, and S. Pinhas, Phys. Rev. B **31**, 6207 (1985)
- [12] R. K. Logan and H. W. Wild, Phys. Rev. **158**, 1467 (1967)
- [13] W.-D. Sheng and J.-B. Xia, J. Phys.: Condens. Matter **8**, 3635 (1996)